AGU PUBLICATIONS

Geophysical Research Letters

RESEARCH LETTER

10.1002/2015GL064029

Key Points:
- Antarctic icequake activity correlates with dominant tide periods
- Observed waveform characteristics can be explained by hybrid event model
- Automatic detection and classification algorithm performs very well

Correspondence to:
C. Hammer,
conny.hammer@sed.ethz.ch

Citation:
Hammer, C., M. Ohrnberger, and V. Schlindwein (2015), Pattern of cryospheric seismic events observed at Ekström Ice Shelf, Antarctica, *Geophys. Res. Lett.*, *42*, doi:10.1002/2015GL064029.

Received 30 MAR 2015
Accepted 16 APR 2015
Accepted article online 23 APR 2015

Pattern of cryospheric seismic events observed at Ekström Ice Shelf, Antarctica

Conny Hammer[1], Matthias Ohrnberger[1], and Vera Schlindwein[2]

[1]Swiss Seismological Service (SED), ETH Zürich, Zürich, Switzerland, [2]Alfred Wegener Institute, Bremerhaven, Germany

Abstract Mobility of glaciers such as rapid retreat or disintegration of large ice volumes produces a large variety of different seismic signals. Thus, evaluating cryospheric seismic events (e.g., changes of their occurrence in space and time) allows to monitor glacier dynamics. We analyze a 1 year data span recorded at the Neumayer seismic network in Antarctica. Events are automatically recognized using hidden Markov models. In this study we focused on a specific event type occurring close to the grounding line of the Ekström ice shelf. Observed waveform characteristics are consistent with an initial fracturing followed by the resonance of a water-filled cavity resulting in a so-called hybrid event. The number of events detected strongly correlates with dominant tide periods. We assume the cracking to be driven by existing glacier stresses trough bending. Voids are then filled by seawater, exciting the observed resonance. In agreement with this model, events occur almost exclusively during rising tides where cavities are opened at the bottom of the glacier, i.e., at the sea/ice interface.

1. Introduction

Cryospheric seismicity reflects a variety of dynamic glacial processes, ranging from ocean-ice interactions to long-term climate change responses. While some common signal types are observed at many glaciers, the source mechanisms are still debated and may vary from glacier to glacier depending on its physical properties. Calving events [e.g., *Qamar*, 1988; *O'Neel et al.*, 2007], sliding at the glacier base [*Deichmann et al.*, 2000; *Zoet et al.*, 2012; *Pratt et al.*, 2014], and ice fracturing [*Neave and Savage*, 1970] produce the most common signals.

While their potential to monitor glacier activity has been recognized widely during the last decades [e.g., *Vanwormer and Berg*, 1973; *Cichowicz*, 1983], the detection of cryospheric seismicity and its discrimination from tectonic seismicity is a difficult task [*Sinadinovski et al.*, 1999]. Human-based perception is practically limited to short observation periods and may be influenced by the subjective view of the analyst. Threshold trigger (i.e., short-term average/long-term average trigger (STA/LTA), see *Withers et al.* [1998] for a review) are unable to discriminate between tectonic and impulsive events of cryogenic origin. *Koehler et al.* [2012] overcome this problem by subsequently applying a self-organizing map algorithm on prior STA/LTA detections. However, STA/LTA trigger and even more sophisticated picking algorithms (e.g., AR picker [*Leonard and Kennett*, 1999]) have their strength in detection of transient signals. Gradual or smoothly changing signals as common for sources that are not related to sudden shear failure but rather to sustained oscillations of fluid-pressure changes are difficult to detect by testing the stationarity of a time series.

Besides the study of *Koehler et al.* [2012] few studies exist to automatically detect seismic activity of cryospheric origin. *O'Neel et al.* [2007] developed a frequency-domain icequake detector for their local study at Columbia glacier. *Sinadinovski et al.* [1999] used certain waveform characteristics (e.g., first arrival, duration, and second phase) to automatically filter icequakes from tectonic events. *Ekström et al.* [2003] found methods to identify long-period seismic signals in teleseismic records. However, most methods are restricted to specific applications or event types. In order to use long-term seismological observatory records for studies of changing glacial seismicity, a robust automated routine that is able to detect and distinguish a variety of different cryospheric signals is needed. High noise levels, variable appearance of seismic signals, and data gaps in polar seismological records pose significant challenges to an automatic event discrimination routine. Hence, applying intelligent algorithms (here hidden Markov model (HMM)) for routinely detecting seismic events of cryospheric origin seems a valuable alternative which we will pursue in this study.

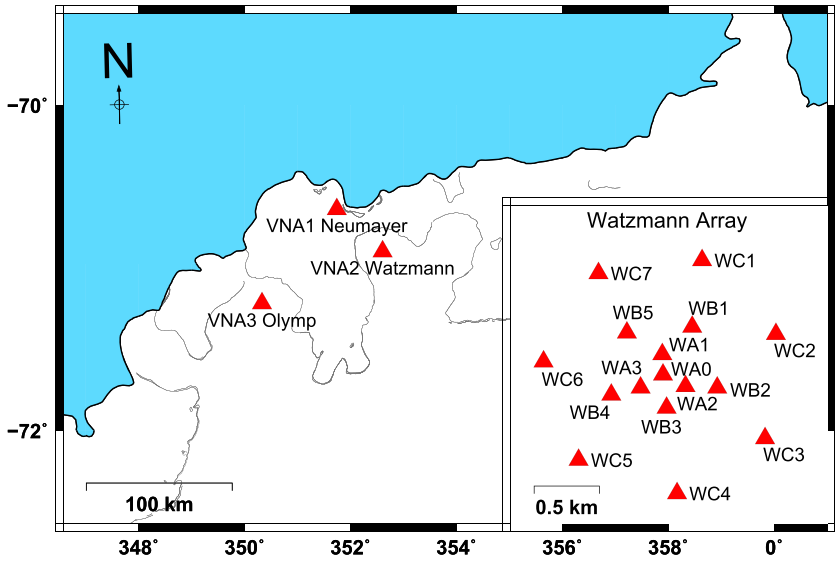

Figure 1. The Neumayer seismological network. The inset shows the geometry of the Watzmann short-period array clustered around station VNA2 (named WA0 in the array). The grey dots indicate the grounding line mapping according to *Rignot et al.* [2012].

HMMs describe highly variable time series by a data-driven stochastic model (see *Rabiner*, [1989] for an overview) and have been successfully applied in seismic signal detection [*Beyreuther et al.*, 2012] and classification [*Benitez et al.*, 2007; *Beyreuther and Wassermann*, 2011]. By using HMMs we identify, classify, and evaluate cryoseismic events for a 1 year data record. In the next sections we give a brief overview of the data set and the used methods followed by a detailed investigation of detected seismic activity. Finally we discuss potential source mechanisms for the observed cryospheric seismicity.

2. Data Set and Methods

We investigate a data set recorded at the Neumayer seismic network (Figure 1) in Antarctica. The network yields continuous seismic records from stations VNA1–VNA3 [*Büßelberg et al.*, 2001]. VNA1 is a short-period, three-component seismograph (Lennartz-5s) situated at the geophysical observatory near Neumayer base on the Ekström Ice Shelf. VNA2 "Watzmann" and VNA3 "Olymp" are intermediate-period three-component sensors (Lennartz-20s, since 2010: broadband (50 Hz-120 s) Guralp sensors) on grounded ice of ice rises 45 km SE and 90 km SW of Neumayer. In addition, VNA2 (named WA0 in the array) is the central sensor of a 16-element short-period, small-aperture array consisting of 15 short-period vertical seismometers arranged on three concentric rings (Figure 1, inset). The total diameter of the outer ring is 1960 m.

Event detection is done automatically on the continuous data streams of the Watzmann array. An initial STA/LTA detection is followed by a frequency-wave number (fk) analysis if predefined trigger criteria are met. However, the automatic routine cannot distinguish between local tectonic events and impulsive events of cryospheric origin. Additionally, events showing emergent onsets might be missed. In the following we investigate continuous data recorded at station WA1 from January to December 2004.

Given a missing classification scheme for local seismicity observed in this vicinity, we first identified interesting events manually on basis of a daily fk analysis. Local and regional seismic events are characterized by lower apparent velocities, i.e., by higher slowness values $p > 0.1$ s/km. The daily fk plot shows two regions of enhanced local activity (Figure 2). Both periods are dominated by a specific type of monochromatic event (Figures 3a and 3b). Corresponding waveforms show a duration of 7 s and slowness values of 0.3 to 0.4 s/km. The dominating frequency covers a very narrow range shifting from 1 Hz in the beginning to 2 Hz at the end of the events. Events cluster in back azimuthal regions of 50°, 230°, and 300°. Considering a station toward the corresponding source region, all signals show frequencies of up to 8 Hz in the beginning (Figures 3a, right, and 3b, right). This is due to attenuation. High frequencies are removed at a faster rate than low frequencies. Thus, high frequencies are only visible at the closest stations. In addition, there are other types of events. Examples are shown in Figure 3d. Such signals might correspond to stranded icebergs [*Müller et al.*, 2005] or

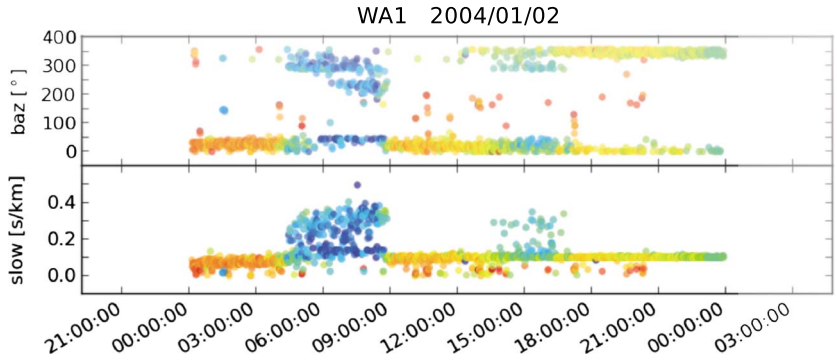

Figure 2. Fk analysis of seismic data recorded at 2 January 2004 at station WA1. (top) The back azimuth and (bottom) the slowness are shown. Colors correspond to values in relative power.

calving at the shelf ice edge. Exact source processes are still unknown. As these events are much rarer in the investigated data set, we focused in the following on the dominant event type described above. A detailed investigation of event types shown in Figure 3d will be subject to future research.

After identifying event classes manually we start the automatic classification procedure. Given the large variability of observed waveforms (Figures 3a and 3b), we use a probabilistic approach which outperforms classical classification techniques such as cross correlation [*Hammer et al.*, 2012, 2013]. Here we provide only a brief overview, see *Hammer et al.* [2013] for a detailed description of the system setup. The classification is not based on the raw waveform directly; thus, the waveform is first "translated" into different wavefield parameters (e.g., spectral features) allowing to better discriminate different seismic signal types. Then for each signal class of interest (e.g., calving event and basal event) and the background noise a generative probabilistic model (here HMM) is learned from prelabeled training data. Providing a prototype for each class of interest, the trained HMM aims to summarize typical class characteristics. Therefore, the number of training samples directly influences the system performance. Until now, there has been no systematic study of cryoseismic events observed at Neumayer seismic network. Hence, a reliable classification scheme as well as a sufficiently large database of preclassified events for learning appropriate prototypes is not available. For that reason we use an approach that requires a minimum amount of training data, i.e., a single reference waveform [*Hammer et al.*, 2012]. The approach allows to construct corresponding classifiers on the fly while enabling the recognition of highly variable time series.

Classifying of unseen data is carried out by first converting short time segments of the continuous waveform into the chosen feature set. Second, computing the likelihood that the observation sequence at hand has been generated by a specific HMM for each individual class HMM and the noise/background HMM. Third, the HMM that best describes the observed feature sequence (i.e., achieving the highest likelihood) is chosen as the winning model. In this way each time instance in the continuous data stream is assigned to one of multiple classes, which can be a specific seismic signal type or noise.

In order to set up a robust classification, we have to construct a background model first. Corresponding parameters are learned from 6 h of continuous background recording capturing both daytime and nighttime. The term background model refers to the intrinsic nature of the model as it captures all "noninteresting" signals (e.g., pure noise but also tectonic events). In the following we make the reasonable assumption that source conditions are the same in summer and winter; thus, event models are fixed over the year. However, noise characteristics in the Antarctic Ocean are subject to daily and seasonal variations [*Grob et al.*, 2011; *Matsumoto et al.*, 2014]. Therefore, the background model needs to be adjusted regularly to actual noise characteristics in order to take all possible variations of class properties into account. However, enriching the training data set might lead to a reduced system performance due to a widening of the noise class. This can be avoided by not running the iterative training cycle until convergence but stopping after few iterations on the most recent data samples [*Riggelsen and Ohrnberger*, 2012]. Alternatively, the earliest training samples might be "forgotten." In this study we follow the second suggestion. Every day we randomly select a period of 15 min every hour to train the background model from scratch.

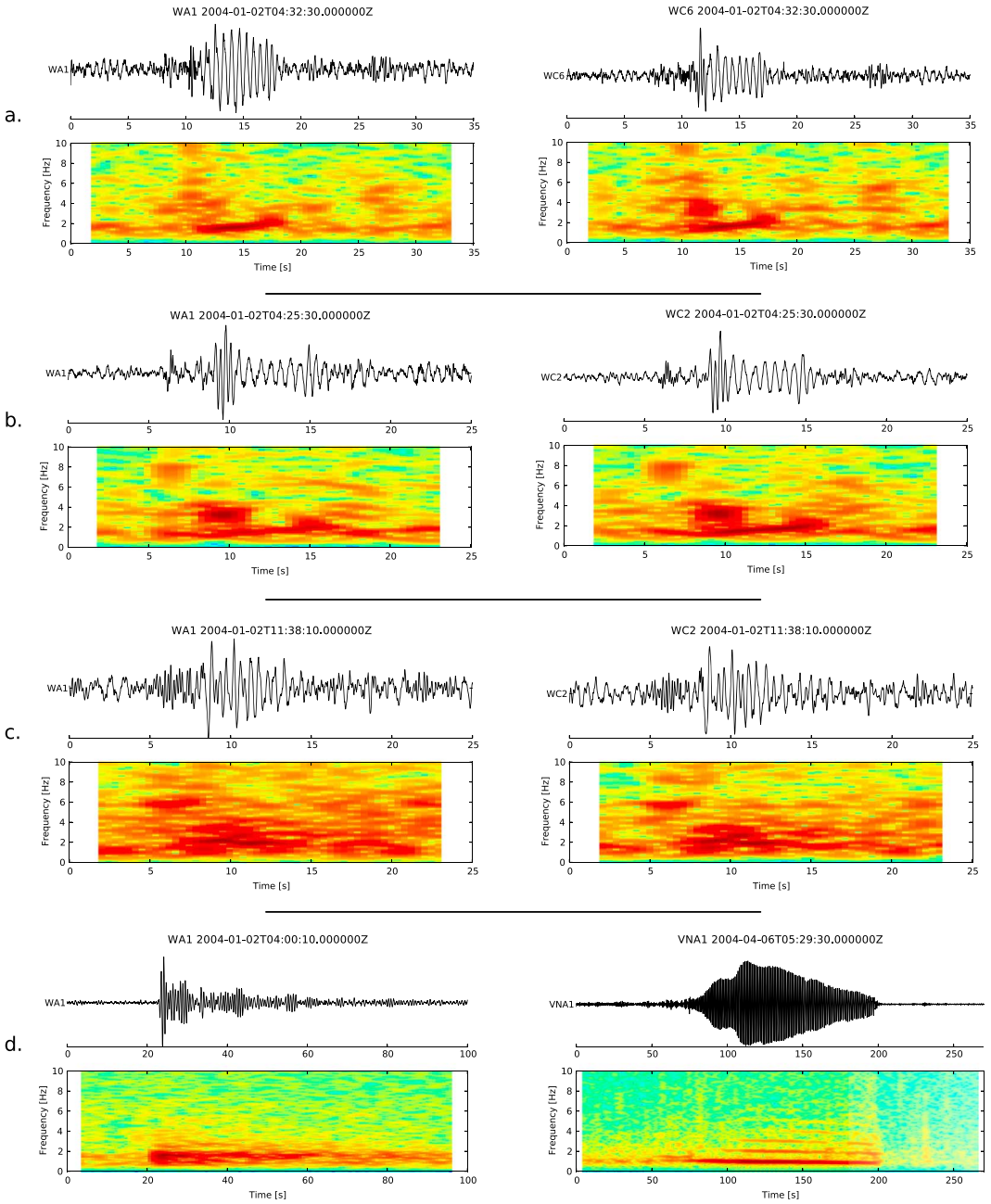

Figure 3. Waveforms and spectrograms of manual identified events. (a–c) An event each recorded at different stations. Figures 3a (back azimuth 300°) and 3b (back azimuth 45°) are recorded during rising tides. Figure 3c is recorded during falling tides. (d) Other event classes manually identified in the observation period. Data are band pass between filtered 0.1 and 25 Hz.

3. Detected Cryoseismic Activity

The hourly occurrence of detected events shows large variations from 0 to 100 events. Detected events in the year 2004 are shown in Figure 4a together with sea level changes. The sea level is calculated with the MATLAB toolbox tidal model driver (written by L. Erofeeva). Here the model CATS02.01 [*Padman et al.*, 2002] is used. CATS02.01 is a medium-resolution (10 km) regional model of the entire circum-Antarctic Ocean and includes ocean cavities under the floating ice shelves.

Figure 4a shows the hourly number of detected events. The number of events is highest in austral spring. The maximum number of events per hour has been detected in October. Even though no data are available from

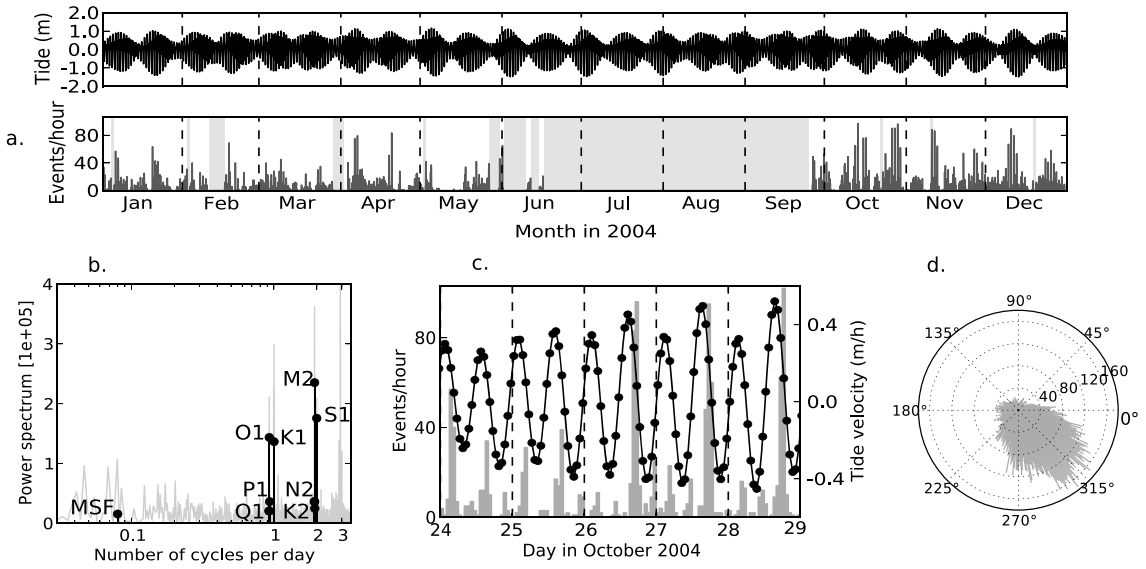

Figure 4. Overview of detections at station WA1. (a) Hourly detected events in 2004 together with (top) sea level change is shown. Light grey periods indicate data gaps, and dark grey bars indicate number of detected events. (b) Periodogram of detected events and tides (complete year 2004). (c) Vertical tide velocity and detected events. (d) Temporal event positions with respect to adjacent maxima in tide (360° apart) are shown (complete year 2004).

mid-June to mid-September the number of events detected suggests a slight seasonal variation. Less events are detected toward autumn, while more events are detected toward spring and summer. Throughout the year there are several days on which no events are detected (e.g., end of January, second half of April, mid-May, and first half of November). Those days cluster in time (i.e., occur in sequence). Moreover, the number of events detected directly correlates with sea level height. The periodogram of hourly detected events shows clear peaks that coincide with dominant tide periods such as the semidiurnal (e.g., M2), diurnal (e.g., K1, P1, and Q1), and forthnightly (e.g., MSF (lunisolar synodic constituent)) tides (Figure 4b). Peaks of higher order are due to overtones [*Kobarg*, 1988]. The comparison of sea level height and hourly detected events shows a correlation between number of events occurring and vertical tide velocity (Figure 4c). Almost all events are observed shortly after the minima and maxima tide velocity (i.e., at rising or falling tides). In addition, Figure 4c suggests a peak shortly after the maximum upward tide velocity, i.e., at rising tides, but a more systematic inspection is needed.

In order to investigate the temporal correlation of event occurrences and sea level, in detail, we use an approach presented by *Heaton* [1975]. The temporal position of events with respect to adjacent maxima in sea level is calculated. Adjacent maxima are defined to be 360° apart; i.e., midfalling and midrising tides are observed at 90° and 270°, respectively. Using this tidal angle representation, any event origin time can be assigned to a specific tidal angle. These tidal angles are then plotted on a rose diagram. Describing the events as a unit vector directed toward the corresponding tidal angle allows to judge on the randomness of the observed pattern. If event origin times and tides are independent, the distribution of tidal angles would be uniform. Following Figure 4d, we find a clear correlation of event occurrence and direction of tide velocity. The rose diagram of tidal angles shows a principal direction of about 315°. Therefore, most of the events occur during rising tides, i.e., shortly after the maximum of upward tide velocity.

4. Discussion and Conclusion

First, we have to evaluate the system performance. False alarms and missing events might distort the actual event pattern. For this reason we investigated 2 January, 11 April, 16 October, and 22 December in detail and picked events manually. For all days the automatic classification routine missed about 7% of the overall number of events and detected about 2% false alarms. In addition, we checked manually 2 days on which no events are detected, 21 March and 8 November. On both days we could confirm the automatic results. Given this match we assume the automatic routine to show the actual pattern of event occurrence.

Few studies report on tidal dependence of icequake occurrence. *Von der Osten-Woldenburg* [1990] and *Barruol et al.* [2013] report on surface crevassing resulting in high-frequency events. Surface crevassing is maximal

at falling tides due to bending along the grounding line. At rising tides events with smaller amplitudes are observed. In addition, *Eckstaller* [1988] describes events also due to bending but with a maximum event occurrence during rising tides. He explained this by the water contact which reduces the fracture strength at the bottom of the ice leading to an increased event occurrence. *Zoet et al.* [2012] also observe tide modulated events. They interpret such highly repetitive waveforms as stick-slip motion at the glacier bed. Being the result of an accelerated ice flow due to a reduced back pressure at the ice front, the number of events in their study is maximal just after low tides. In our study the number of events is maximal between midrising and high tides. This disagrees with a basal seismicity due to ice moving over the underlying bedrock. During high tides the back pressure at the ice front is maximal. That reduces the flow speed and would lead to a decreasing number of events. Moreover, at high tides the friction between ice and underlying bedrock is lowest, which would also reduce the number events occurring. Therefore, we do not consider the hypothesis of gliding at the glacier base in this study.

Low-frequency, monochromatic events are consistent with signals generated from stick-slip motions at the glacier bed [*MacAyeal et al.*, 2008] or from pressure transients in fluid-filled cavities [e.g., *Métaxian et al.*, 2003; *West et al.*, 2010]. As explained before we follow the second idea. The resonance excited on the crack walls propagates through the ice producing the observed waveforms. Here various scenarios are conceivable. Either water penetrates into the glacier and drives the expansion of existing cracks followed by the rush of water into the new opening or water is forced through the narrowing of already existing cracks [*O'Neel and Pfeffer*, 2007]. In both scenarios event occurrence is driven by water pressure. Alternatively, events might be driven by fracturing due to glacier stresses [*West et al.*, 2010]. In this model water is drawn to fill the stress-induced opening resulting in a resonating system. *West et al.* [2010] relate this process to so-called hybrid events. These events have high-frequency onsets followed by a low-frequency coda which implies an initial stress-induced fracturing followed by a fluid-induced resonance.

The tidal dependence observed in this study contradicts the triggering by water pressure only. This fact as well as the high-frequency beginning of the events (Figures 3a and 3b) leads us to conclude that we are dealing with hybrid events. We propose the following model. Near the grounding line ice masses are partly floating on the sea and partly lying on the bedrock. The floating part is subject to vertical tidal movements generating an extensive state of stress within the ice tongue along the grounding line. The entailed stress reduction then induces fracturing at the top or bottom of the glacier depending on the direction of the bending (e.g., rising or falling tides). Then water runs into the new void stimulating the crack walls to resonate. The ice of the Ekström Ice Shelf is always below freezing point from the surface to its base. This prevents the existence of meltwater. Hence, we assume another source of necessary fluids for the proposed model. The floating part of the glacier is surrounded by water at its lower part. Open cavities will be filled by inflowing seawater exciting the observed resonance.

This model is supported by various facts, first the temporal position of event occurrences. While the bending is likely to be active at both rising and falling tides the number of events observed differs significantly. The maximum number of events is observed between low and high tides, i.e., at rising tides (Figure 4d). At this time fractures are induced at the bottom of the glacier. In contrast, considerably less events are observed during falling tides, on which fractures are expected at the surface of the glacier. This is consistent with the proposed model: While the sea/ice interface at the bottom provides conditions for event generation, events are missing at the ice/snow interface. Consequently, downward bending induces fracturing at the surface of the glacier but no resonance is excited. As the resonance part (i.e., the monochromatic part about 1 to 2 Hz) is a significant component of the classifier trained at station WA1 no events are detected during falling tides. The few events detected during falling tides show a much less pronounced resonance part (Figure 3c).

Another indication for the proposed model is the location of the events. Based on the model the location of events corresponds to the location of the grounding line. Considering the stronger attenuation of high frequencies the grounding line toward NW should be farther away than toward NE and SW. This is in agreement with the grounding line mapping of *Rignot et al.* [2012] (Figure 1). According to this the grounding line is 22.5 km and 18.0 km away from station WA1.

Finally observed waveform characteristics are consistent with the proposed model. In resonant systems the characteristic frequency depends on the resonator geometry. *O'Neel and Pfeffer* [2007] showed that fundamental mode frequencies of 1 to 3 Hz might be produced by reasonable crack dimensions of width <1 m and

length < ice thickness. Basal crevasses up to hundreds of meters in height have been identified in the flanking Fimbul Ice Shelf [*Humbert and Steinhage*, 2011].

However, neither the days without any event nor the variations throughout the year can be explained by this model. Variations in event occurrence may be due to different reasons. Either events are existent but covered by a dominating background noise (e.g., due to wind direction and/or velocity) or additional factors affect the triggering of events. Changes in the bending alter the number of detected events. There is a variety of forces that can enhance or mitigate the tidal bending, ranging from ocean swell to atmospheric factors such as wind and barometric pressure [*Goodman et al.*, 1980; *Kobarg*, 1988]. In addition, there are nonbending related factors such as modified failure conditions at the bottom of the glacier. Increasing temperatures of seawater decreases the fracture strength [*Petrovic*, 2003]. In addition, warmer seawater prevents the fractures to heal completely. Thus, resonance will be generated by already existing and new cracks. Both effects result in an increase in event occurrence. The detailed analysis of all these factors as well as their impact on event occurrence will be subject to future research. In combination with an expansion of the classification system to other event types and the processing of larger observation periods we hope to shed some light on current glacier dynamics in Antarctica.

Acknowledgments

This work was supported by the Deutsche Forschungsgemeinschaft (DFG) in the framework of the priority programme "Antarctic Research with comparative investigations in Arctic ice areas" by a grant (project ICE-quakes, contracts OH 90/2-1 and SCHL 853/2-1). Constructive reviews by two anonymous reviewers greatly improved this manuscript. Data are freely available and can be obtained via GFZ Potsdam (www.geofon.gfz-potsdam.de).

The Editor thanks two anonymous reviewers for their assistance in evaluating this paper.

References

Barruol, G., E. Cordier, J. Bascou, F. R. Fontaine, B. Legresy, and L. Lescarmontier (2013), Tide-induced microseismicity in the Mertz glacier grounding area, East Antarctica, *Geophys. Res. Lett.*, *40*, 5412–5416, doi:10.1002/2013GL057814.

Benitez, M. C., J. Ramirez, J. C. Segura, J. M. Ibanez, J. Almendros, A. Garcia-Yeguas, and G. Cortes (2007), Continuous HMM-based seismic-event classification at Deception Island, Antarctica, *IEEE Trans. Geosci. Remote Sens.*, *45*(1), 138–146, doi:10.1109/TGRS.2006.882264.

Beyreuther, M., and J. Wassermann (2011), Hidden semi-Markov model based earthquake classification system using weighted finite-state transducers, *Nonlinear Processes Geophys.*, *18*, 81–89, doi:10.5194/npg-18-81-2011.

Beyreuther, M., C. Hammer, J. Wassermann, M. Ohrnberger, and T. Megies (2012), Constructing a hidden Markov model based earthquake detector: Application to induced seismicity, *Geophys. J. Int.*, *189*(1), 602–610, doi:10.1111/j.1365-246X.2012.05361.x.

Büßelberg, T., C. Müller, and A. Eckstaller (2001), The Neumayer array and its impact on seismological research in the South Atlantic and Antarctica, *Terra Antartica*, *8*(2), 41–48.

Cichowicz, A. (1983), Icequakes and glacier motion: The Hans glacier, Spitsbergen, *Pure Appl. Geophys.*, *121*(1), 27–38.

Deichmann, N., J. Ansorge, F. Scherbaum, A. Aschwanden, F. Bernardi, and G. Gudmundsson (2000), Evidence for deep icequakes in an Alpine glacier, *Ann. Glaciol.*, *31*, 85–90, doi:10.3189/172756400781820462.

Eckstaller, A. (1988), Seismologische Untersuchungen mit Daten der Georg-von-Neumayer Station, Antarktis, 1982–1984, PhD thesis, Ludwig-Maximilians- Universität, München, German.

Ekström, G., M. Nettles, and G. Abers (2003), Glacial earthquakes, *Science*, *302*(5645), 622–624, doi:10.1126/science.1088057.

Goodman, D., P. Wadhams, and V. Squire (1980), The flexural response of a tabular ice island to ocean swell, *Ann. Glaciol.*, *1*, 23–27.

Grob, M., A. Maggi, and E. Stutzmann (2011), Observations of the seasonality of the Antarctic microseismic signal, and its association to sea ice variability, *Geophys. Res. Lett.*, *38*, L11302, doi:10.1029/2011GL047525.

Hammer, C., M. Beyreuther, and M. Ohrnberger (2012), A seismic-event spotting system for volcano fast-response systems, *Bull. Seismol. Soc. Am.*, *3*, 948–960, doi:10.1785/0120110167.

Hammer, C., M. Ohrnberger, and D. Faeh (2013), Classifying seismic waveforms from scratch: A case study in the alpine environment, *Geophys. J. Int.*, *192*(1), 425–439, doi:10.1093/gji/ggs036.

Heaton, T. (1975), Tidal triggering of earthquakes, *Geophys. J. R. Astron. Soc.*, *43*(2), 307–326, doi:10.1111/j.1365-246X.1975.tb00637.x.

Humbert, A., and D. Steinhage (2011), The evolution of the western rift area of the Fimbul Ice Shelf, Antarctica, *Cryosphere*, *5*(4), 931–944, doi:10.5194/tc-5-931-2011.

Kobarg, W. (1988), Die gezeitenbedingte dynamik des ekström-schelfeises, antarktis = the tide-dependent dynamics of the Ekström Ice Shelf, Antarctica, *Berichte zur Polarforschung (Reports on Polar Research)*, vol. 50, 164 pp., Alfred Wegener Inst. for Polar and Mar. Rese., Bremerhaven, German.

Koehler, A., A. Chapuis, C. Nuth, J. Kohler, and C. Weidle (2012), Autonomous detection of calving-related seismicity at Kronebreen, Svalbard, *Cryosphere*, *6*(2), 393–406, doi:10.5194/tc-6-393-2012.

Leonard, M., and B. Kennett (1999), Multi-component autoregressive techniques for the analysis of seismograms, *Phys. Earth Planet. Inter.*, *113*(1–4), 247–263.

Matsumoto, H., D. R. Bohnenstiehl, J. Tournadre, R. P. Dziak, J. H. Haxel, T. K. A. Lau, M. Fowler, and S. A. Salo (2014), Antarctic icebergs: A significant natural ocean sound source in the Southern Hemisphere, *Geochem. Geophys. Geosyst.*, *15*, 3448–3458, doi:10.1002/2014GC005454.

MacAyeal, D. R., E. A. Okal, R. C. Aster, and J. N. Bassis (2008), Seismic and hydroacoustic tremor generated by colliding icebergs, *J. Geophys. Res.*, *113*, F03011, doi:10.1029/2008JF001005.

Métaxian, J.-P., S. Araujo, M. Mora, and P. Lesage (2003), Seismicity related to the glacier of Cotopaxi Volcano, Ecuador, *Geophys. Res. Lett.*, *30*(9), 1483, doi:10.1029/2002GL016773.

Müller, C., V. Schlindwein, A. Eckstaller, and H. Miller (2005), Singing icebergs, *Science*, *310*(5752), 1299.

Neave, K., and J. Savage (1970), Icequakes on Athabasca Glacier, *J. Geophys. Res.*, *75*(8), 1351–1362, doi:10.1029/JB075i008p01351.

O'Neel, S., and W. T. Pfeffer (2007), Source mechanics for monochromatic icequakes produced during iceberg calving at Columbia Glacier, AK, *Geophys. Res. Lett.*, *34*, L22502, doi:10.1029/2007GL031370.

O'Neel, S., H. P. Marshall, D. E. McNamara, and W. T. Pfeffer (2007), Seismic detection and analysis of icequakes at Columbia Glacier, Alaska, *J. Geophys. Res.*, *112*, F03S23, doi:10.1029/2006JF000595.

Padman, L., H. Fricker, R. Coleman, S. Howard, and L. Erofeeva (2002), A new tide model for the Antarctic ice shelves and seas, *Ann. Glaciol.*, *34*, 247–254, doi:10.3189/172756402781817752.

Pratt, M. J., J. P. Winberry, D. A. Wiens, S. Anandakrishnan, and R. B. Alley (2014), Seismic and geodetic evidence for grounding-line control of Whillans Ice Stream stick-slip events, *J. Geophys. Res. Earth Surf.*, *119*, 333–348, doi:10.1002/2013JF002842.

Petrovic, J. (2003), Review mechanical properties of ice and snow, *J. Mater. Sci.*, *38*(1), 1–6.

Qamar, A. (1988), Calving icebergs—A source of low-frequency seismic signals from Columbia glacier, Alaska, *J. Geophys. Res.*, *93*(B6), 6615–6623, doi:10.1029/JB093iB06p06615.

Rabiner, L. (1989), A tutorial on hidden Markov models and selected applications in speech recognition, *Proc. IEEE*, *77*(2), 257–286.

Riggelsen, C., and M. Ohrnberger (2012), A machine learning approach for improving the detection capabilities at CTBTO/IMS 3C seismic stations, *Pure Appl. Geophys.*, *171*, 395–411, doi:10.1007/s00024-012-0592-3. Special issue: Recent Advances in Nuclear Explosion.

Rignot, E., J. Mouginot, and B. Scheuchl (2011), Antarctic grounding line mapping from differential satellite radar interferometry, *Geophys. Res. Lett.*, *38*, L10504, doi:10.1029/2011GL047109.

Sinadinovski, C., K. Muirhead, M. Leonard, S. Spiliopoulos, and D. Jespen (1999), Effective discrimination of icequakes on seismic records from Mawson station, *Phys. Earth Planet. Inter.*, *113*(1–4), 203–211, doi:10.1016/S0031-9201(99)00005-9.

Vanwormer, D., and E. Berg (1973), Seismic evidence for glacier motion, *J. Glaciol.*, *12*, 259–265.

von der Osten-Woldenburg, H. (1990), Icequakes on Ekström Ice Shelf near Atka Bay, Antarctica, *J. Glaciol.*, *36*(122), 31–36.

West, M. E., C. F. Larsen, M. Truffer, S. O'Neel, and L. LeBlanc (2010), Glacier microseismicity, *Geology*, *38*(4), 319–322, doi:10.1130/G30606.1.

Withers, M., R. Aster, C. Young, J. Beiriger, M. Harris, S. Moore, and J. Trujillo (1998), A comparison of select trigger algorithms for automated global seismic phase and event detection, *Bull. Seismol. Soc. Am.*, *88*(1), 95–106.

Zoet, L. K., S. Anandakrishnan, R. B. Alley, A. A. Nyblade, and D. A. Wiens (2012), Motion of an Antarctic glacier by repeated tidally modulated earthquakes, *Nat. Geosci.*, *5*(9), 623–626, doi:10.1038/NGEO1555.